Available online at www.sciencedirect.com
ScienceDirect
Journal of Crystal Growth 310 (2008) 2330–2333
JOURNAL OF CRYSTAL GROWTH
www.elsevier.com/locate/jcrysgro

Characteristics of ultraviolet nonpolar InGaN/GaN light-emitting diodes using trench epitaxial lateral overgrowth technology

Shih-Chun Ling, Te-Chung Wang, Tsung-Shine Ko, Tien-Chang Lu*, Hao-Chung Kuo*, Shing-Chung Wang

Department of Photonics & Institute of Electro-Optical Engineering, National Chiao Tung University, 1001 Ta Hsueh Road, Hsinchu 300, Taiwan

Available online 14 December 2007

Abstract

Ultraviolet nonpolar InGaN/GaN light-emitting diodes grown on trench epitaxial lateral overgrowth (TELOG) *a*-plane GaN template by metalorganic chemical vapor deposition were fabricated. Two emission peaks at 373 and 443 nm are observed from each fabricated device. The double emission peaks feature is identified by cathodoluminescence images, which show that the ultraviolet peak is emitted from the low-defect density wings on the TELOG and the blue peak is emitted from the TELOG-coalesced seed areas due to different incorporation of indium. The *L–I–V* diagram revealed that there are leakage current pathways due to the many threading dislocations in seed regions, and that the output power reached 0.2 mW at 140 mA. Two electroluminescence (EL) peaks are observed simultaneously when the driving current is below 50 mA. However, the EL peak at 373 nm dominates when current is above 50 mA. In addition, the degree of polarization of the ultraviolet peak was measured and found to be 28.7%.

PACS: 85.60.Jb; 81.15.Gh; 61.66.Fn

Keywords: A3. Metalorganic chemical vapor deposition; B1. Inorganic compounds; B2. Semiconducting gallium compounds; B3. Light emitting diodes

1. Introduction

Recently, ultraviolet light-emitting diodes (UV LEDs) have been attracting great attention since they could be used to fabricate white LEDs. Such an approach has the advantage that color can be controlled by the phosphor mix at one point, so color rendering will be excellent [1]. However, the conventional *c*-plane UV LEDs suffer from the quantum-confined Stark effect [2,3], due to the existence of strong piezoelectric and spontaneous polarizations [4]. The built-in electric fields along the *c*-direction cause spatial separation of electrons and holes, which gives rise to restricted carrier recombination efficiency, reduced oscillator strength, and red-shifted emission [5].

Since the performance of III-nitride LEDs are limited by the polarization-related internal electric fields, nonpolar *a*-plane LEDs are currently the subject of intense research to improve the internal quantum efficiency [6,7]. Unfortunately, nonpolar *a*-plane GaN-based material grown on *r*-plane sapphire substrates always shows wavy, stripe-like growth features and possesses a large density of threading dislocations (TDs) (10^9–$10^{10}\,cm^{-2}$) and stacking faults [8]. The high defect density in the GaN films limits the LED performance because TDs act as nonradiative centers and reduce radiative recombination efficiency. In addition, the lattice mismatch between the *a*-plane GaN and *r*-plane sapphire results in a serious anisotropic in-plane strain difference between orthogonal crystal axes [9]. Therefore, we have proposed an approach to improve [1 1 $\bar{2}$ 0] *a*-plane GaN quality by using epitaxial lateral overgrowth on trenched *a*-plane GaN buffer layers [10]. The trenched epitaxial lateral overgrowth (TELOG) allowed us to obtain *a*-plane GaN with low dislocation density, simple fabrication process, lower cost, and thinner coalescence thickness in comparison with previous reports [11,12]. The research on *a*-plane InGaN/GaN LEDs has been focusing on the

*Corresponding authors. Tel.: +886 3 5712121; fax: +886 3 5716631.
E-mail addresses: timtclu@faculty.nctu.edu.tw (T.-C. Lu), hckuo@faculty.nctu.edu.tw (H.-C. Kuo).

0022-0248/$ - see front matter © 2008 Elsevier B.V. All rights reserved.
doi:10.1016/j.jcrysgro.2007.12.013

blue emission range for many years. In this study, we report on the fabrication of UV nonpolar InGaN/GaN LEDs using a reduced-defect trench epitaxial lateral overgrowth *a*-plane GaN template and discuss characteristics of these devices.

2. Experiments

First, *a*-plane GaN films with 1.5 μm thickness were grown by low-pressure metal-organic chemical vapor deposition (MOCVD) on *r*-plane sapphire substrates using conventional two-step growth technique. Then, SiO_2 was deposited and patterned to realize a 2 μm seed/7 μm trench TELOG stripe pattern parallel to the $[1\ \bar{1}\ 0\ 0]$ direction (to obtain vertical *c*-plane sidewalls). SiO_2 was etched using inductively coupled plasma etching through the windows to the GaN epitaxial film. The GaN in the trench areas (unprotected by SiO_2) was etched by reactive-ion etching down to the *r*-plane sapphire substrate. The SiO_2 mask was removed by hydrofluoric acid to simplify the growth process. We then continue to perform the regrowth process on 2 μm seed/7 μm trench stripe patterns to obtain a fully coalesced *a*-plane GaN template [10]. Later, the LED structure was regrown by MOCVD on the *a*-plane TELOG GaN template.

Fig. 1 shows the structure of the UV nonpolar TELOG LED. It consisted of 12-μm-thick TELOG GaN template, a 1.5-μm-thick Si-doped n-GaN with an electron concentration of $3\times10^{18}\,cm^{-3}$, a 0.1-μm-thick n-GaN with an electron concentration of $1\times10^{18}\,cm^{-3}$, followed by the active region, which consisted of eight pairs of MQWs with 15-nm-thick GaN barriers and 5-nm-thick InGaN wells. A 30-nm-thick p-type $Al_{0.1}Ga_{0.9}N$ electron blocking layer separated the active region from the 0.16-μm-thick p-type GaN with a hole concentration of $6\times10^{17}\,cm^{-3}$. After MOCVD growth, the LED wafer was partially etched by reactive-ion etching from the surface of the p-type GaN until the n-type GaN was exposed. Ni/Au contact metal layers were evaporated onto the p-type GaN contact layer, and a titanium/aluminum (Ti/Al) contact was evaporated onto the n-type GaN layer. The comparison of surface morphologies and defect distributions over various areas were obtained by using scanning electron microscopy (SEM) and spatially resolved cathodoluminescence (CL). The LED spectrum and the degree of polarization were measured by electroluminescence (EL).

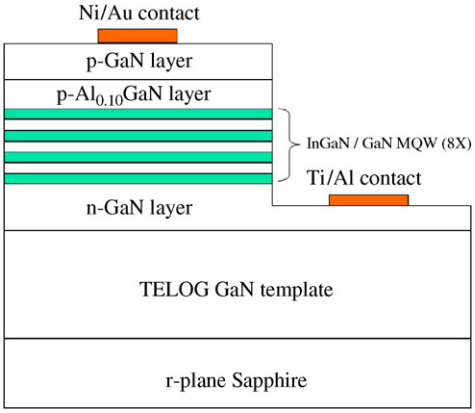

Fig. 1. Structure of the ultraviolet nonpolar TELOG LED.

3. Results and discussion

Fig. 2 shows the cross-sectional SEM image of the *a*-plane UV LED grown on TELOG substrate. Most TDs were located on the GaN seed stripes: they originated from the GaN seed and penetrated through the MQWs to the p-type GaN surface where they were visible as surface pits. The TD density of the GaN wing region was much lower than that of the seed region. Fig. 3(a) shows a plan-view SEM image of a wing with seed regions. Fig. 3(b, c) are the monochromatic CL images of Fig. 3(a) at 373 and 443 nm, respectively. The bright regions showed that the emission of 373 nm mainly came from the low defect density wings. In comparison, the emission of 443 nm came from the high defect density GaN seeds. A similar behavior was observed in the lateral epitaxially overgrown window and wing regions by Chakraborty et al. [13]. They assumed that the presence of defects led to increase in indium incorporation in the poor quality region. We thus suggest that more indium atoms could be incorporated in the MQWs of seed regions with higher dislocation density, resulting in longer-emission wavelength from those areas.

Fig. 4(a) shows the *L–I–V* characteristics of nonpolar TELOG LEDs. The *I–V* curve of the diode showed that the series resistance was about 50 Ω and the forward voltage was below 2 V. This indicated that there could be some leakage current pathways. According to Kozodoy's report [14], we suggest that leakage current pathways could be present due to the high density of TDs in the seed regions. Besides, the output power increased appreciably when the injection current increased over 40 mA and finally reached 0.2 mW at 140 mA. Fig. 4(b) presents the normalized EL

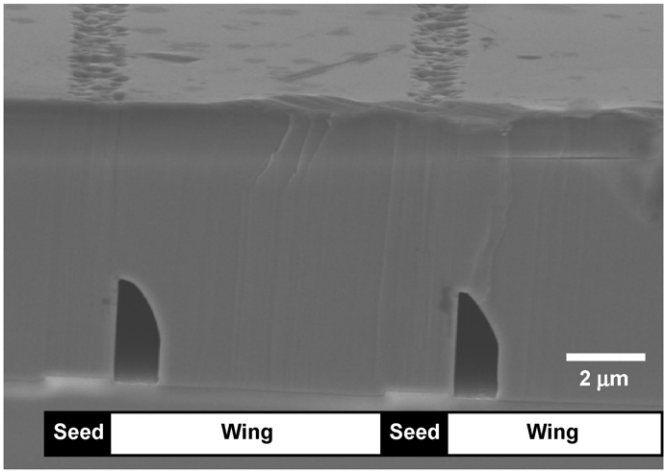

Fig. 2. Cross-sectional SEM image of a TELOG *a*-plane LED with 2 μm seed/7 μm trench patterns.

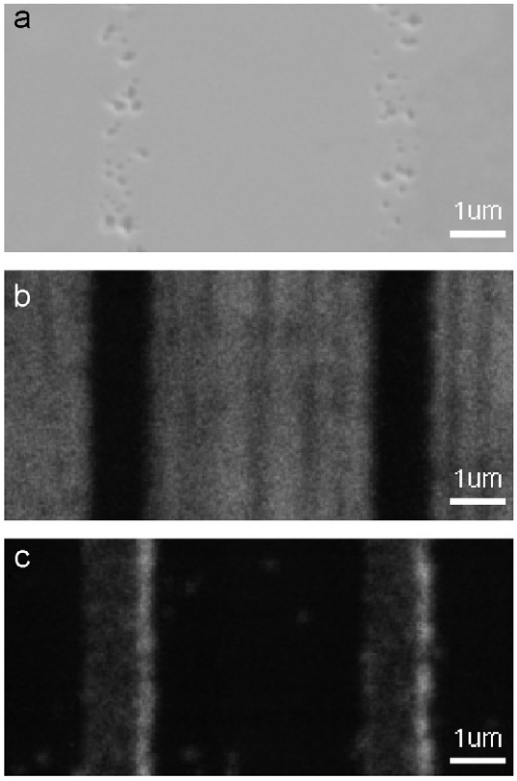

Fig. 3. (a) Plan-view SEM image, including seed regions and wing regions (b) monochromatic CL image at 373 nm and (c) monochromatic CL image at 443 nm.

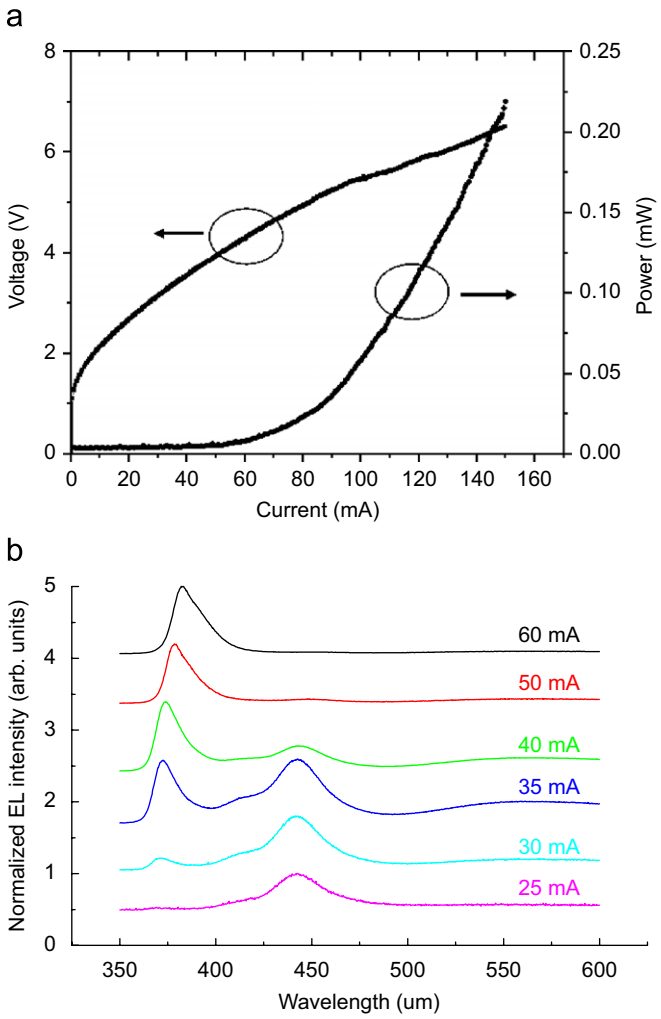

Fig. 4. (a) *L–I–V* characteristics of the ultraviolet nonpolar LED and (b) normalized CW electroluminescence spectra.

spectra at drive currents ranging from 25 to 60 mA. When the injection current was below 25 mA, the spectrum was dominated by the blue emission at 443 nm. Once the current increased over 30 mA, the UV emission at 373 nm appeared in addition to the 443 nm emission. The intensity of the 373 nm UV peak increased much faster than that of the 443 nm UV peak from 30 to 60 mA, and finally the UV peak became the dominant peak. Meanwhile, the 373 nm peak exhibited a red-shift to 382 nm when the current was increased from 30 to 60 mA. This could be attributed to the bandgap shrinkage due to the thermal effect. We assume that the 373 nm UV emission comes from the GaN wing regions as shown in Fig. 3(b). On the other hand, the longer 443 nm wavelength EL emission (bright bands in Fig. 3(c)) comes from the TELOG seed regions. There are two reasons that could account for the special double peaks feature in the EL spectra. First, since many TDs in the seed regions would form leakage current pathways, injection current tends to bypass wing regions and a flow through these leakage channels in the seed regions at an early stage (when the injection current was below 30 mA). The other reason is that the difference of bandgap between the seed and wing regions due to the different indium incorporation that caused different turn-on voltages. Obviously, the turn-on voltage in wing regions was higher than that in the seed regions. Therefore, the injection current preferred to pass through seed regions until the injection current is high enough to spread into wing regions. As a result, the emission peak of 443 nm was the dominant peak at low-injection current and subsequently the 373 nm peak quickly increased in intensity once the injection current spread into the wing regions.

Nonpolar GaN films have been shown to exhibit optically polarized spontaneous emission, which is explained by the crystal field oriented along the *c*-axis of wurtzite GaN and its effect on the valence-band splitting induced by large compressive strain within the wells [15]. The linear polarization of the EL of our devices at room temperature was analyzed by rotating a polarizer between a polarization angle of 0° (referred to as parallel to the *c*-axis) and 360°. The polarization ratio is defined as $\rho = (I_{max}-I_{min})/(I_{max}+I_{min})$, where I_{max} is the intensity of light with polarization perpendicular to the *c*-axis and I_{min} is the intensity of light with polarization parallel to the *c*-axis. Fig. 5 shows the EL intensity of UV spectral range at different polarization angles at room temperature, as the operation current is 80 mA. The degree of polarization is estimated to be about 28.7%. This polarization ratio is lower than that reported at 10 K for the *m*-plane

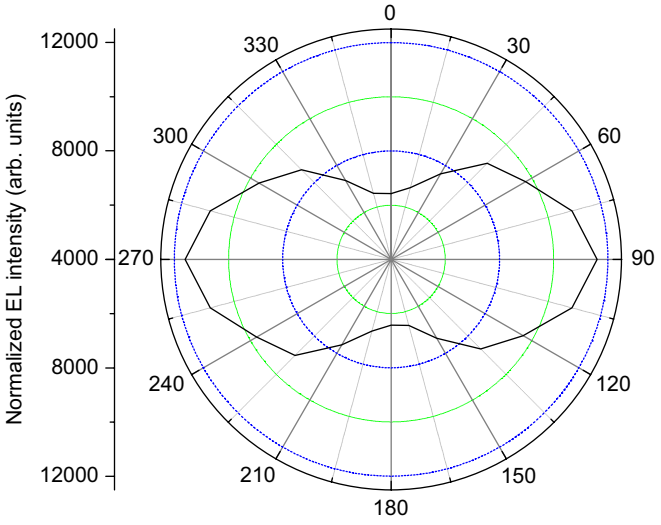

Fig. 5. Polarization degree of the UV spectral range at the operation current of 80 mA.

InGaN/GaN quantum wells grown by molecular beam epitaxy [16]. This could be explained that an increase in device temperature is first due to the ambient temperature and then by current injection and consequently the higher-energy valence band minimum with polarization parallel to the *c*-axis filled with holes, or by population of the valence band from the minimum up to higher energy levels as the hole density increases with forward bias [17].

4. Summary

In conclusion, we have grown nonpolar InGaN/GaN UV LEDs using the TELOG technique. Our CL results revealed that the low defect density wings emitted a 373 nm peak and the TELOG-coalesced seed regions emitted at 443 nm. This difference in emission wavelength is attributed to different incorporation of indium, which was apparently related with the distribution of TDs. The *L–I–V* diagram revealed that the series resistance was about 50 Ω and that there are leakage current pathways due to high density of TDs in seed regions. The EL spectra showed that the peak at 443 nm appeared at first and then the peak of 373 nm was emitted with an increasing current. We proposed that the reasons for this phenomenon were the differences in crystal quality and bandgap between the seed regions and the wing regions. The polarization measurements showed that such LEDs possess 28.7% polarization degree.

Acknowledgment

This work was supported by the MOE ATU program and in part by the National Science Council in Taiwan under Contract nos. NSC 95-2120-M-009-008, NSC 95-2752-E-009-007-PAE, and NSC 95-2221-E-009-282.

References

[1] D.A. Steigerwald, J.C. Bhat, D. Collins, R.M. Fletcher, M.O. Holcomb, M.J. Ludowise, P.S. Martin, S.L. Rudaz, Member IEEE, IEEE J. Sel. Top. Quant. Electron. 8 (2) (2002).
[2] T. Takeuchi, S. Sota, M. Katsuragawa, M. Komori, H. Takeuchi, H. Amano, I. Akasaki, Jpn. J. Appl. Phys. Part 2 36 (1997) L382.
[3] D.A.B. Miller, D.C. Chemla, T.C. Damen, A.C. Grossard, W. Wiegmann, T.H. Wood, C.A. Burrus, Phys. Rev. B 32 (1985) 1043.
[4] F. Bernardini, V. Fiorentini, D. Vanderbilt, Phys. Rev. B 56 (1997) R10024.
[5] J.S. Im, H. Kollmer, J. Off, A. Sohmer, F. Scholz, A. Hangleiter, Phys. Rev. B 57 (1998) R9435.
[6] F. Bernardini, V. Fiorentini, D. Vanderbilt, Phys. Rev. B 56 (1997) R10024.
[7] A. Chakraborty, B.A. Haskell, S. Keller, J.S. Speck, S.P. DenBaars, S. Nakamura, U.K. Mishraa, Appl. Phys. Lett. 85 (22) (2004) 29.
[8] M.D. Craven, S.H. Lim, F. Wu, J.S. Speck, S.P. DenBaars, Appl. Phys. Lett. 81 (2002) 469.
[9] H. Wang, C. Chen, Z. Gong, J. Zhang, M. Gaevski, M. Su, J. Yang, M.A. Khan, Appl. Phys. Lett. 84 (2004) 499.
[10] T.C. Wang, T.C. Lu, T.S. Ko, H.C. Kuo, M. Yu, S.C. Wang, Appl. Phys. Lett. 89 (2006) 251109.
[11] B.A. Haskell, F. Wu, M.D. Craven, S. Matsuda, P.T. Fini, T. Fujii, K. Fujito, S.P. DenBaars, J.S. Speck, S. Nakamura, Appl. Phys. Lett. 83 (4) (2003) 28.
[12] A. Chakraborty, K.C. Kim, F. Wu, J.S. Speck, S.P. DenBaars, U.K. Mishra, Appl. Phys. Lett. 83 (2006) 041903.
[13] A. Chakraborty, S. Keller, C. Meier, S. Nakamura, J.S. Speck, U.K. Mishraa, Appl. Phys. Lett. 86 (2005) 031901.
[14] P. Kozodoy, J.P. Ibbetson, H. Marchand, P.T. Fini, S. Keller, J.S. Speck, S.P. DenBaars, U.K. Mishra, Appl. Phys. Lett. 73 (1998) 975.
[15] B. Rau, P. Waltereit, O. Brandt, M. Ramsteiner, K.H. Ploog, J. Puls, F. Henneberger, Appl. Phys. Lett. 77 (2000) 3343.
[16] Y.J. Sun, O. Brandt, M. Ramsteiner, H.T. Grahn, K.H. Ploog, Appl. Phys. Lett. 82 (2003) 3850.
[17] N.F. Gardner, J.C. Kim, J.J. Wierer, Y.C. Shen, M.R. Krames, Appl. Phys. Lett. 86 (2005) 111101.